

Möbius carbon nanobelts interacting with heavy metal nanoclusters

C. Aguiar¹, N. Dattani^{2,3}, I. Camps^{1,3*}

¹*Laboratório de Modelagem Computacional - LaModel, Instituto de Ciências Exatas - ICEx. Universidade Federal de Alfenas - UNIFAL-MG, Alfenas, Minas Gerais, Brasil*

²*HPQC College, Waterloo, Canada*

³*HPQC Labs, Waterloo, Canada*

Abstract

To investigate the interaction between carbon and Möbius-type carbon nanobelts and nickel, cadmium, and lead nanoclusters, we utilized the semiempirical tight binding framework provided by xTB software. Through our calculations, we determined the lowest energy geometries, complexes stability, binding energy, and electronic properties. Our findings demonstrate that heavy metal nanoclusters have a favorable binding affinity towards both nanobelts, with the Möbius-type nanobelt having a stronger interaction. Additionally, our calculations reveal that the nickel nanocluster has the lowest binding energy, displaying the greatest charge transfer with the nanobelts, which was nearly twice that of the cadmium and lead nanoclusters.

The molecular dynamic simulation showed that all complexes were stable at 298 K, with low root-mean-square deviation and negative binding energy. Homogeneous distribution of the frontier orbitals throughout the nanobelt structure was observed, with slight changes noted in the distribution when the structure was twisted to create the Möbius-type nanobelt. Furthermore, the topological study demonstrated that although the number of bonds between the metal nanoclusters and the Möbius-type nanobelt were the same, the bond intensities were notably different. Bonds formed with the nickel nanocluster were stronger than those formed with cadmium and lead metals. Our combined results lead to the conclusion that the nickel nanoclusters are chemisorbed, whereas cadmium and lead nanoclusters are physisorbed in both nanobelts.

Keywords: heavy metals, carbon nanobelt, Möbius belt, Nickel, Cadmium, Lead

1. Introduction

In recent years, major concerns have been raised about pollution caused by heavy metals resulting from industrialization and daily release into the environment [1; 2]. Improper disposal of these metals can cause numerous diseases [3; 4] and harmful effects on nature [2; 5]. Among the heavy metals commonly found in industrial wastewater are Pb^{2+} , Cd^{2+} , and Ni^{2+} , which have already demonstrated high levels of toxicity [6]. Unlike organic compounds, heavy metals are not biodegradable, so there is no natural degradation, and they have been observed in living organisms' tissues and damaged gills of some fish [2; 7; 8].

Therefore, new studies have been developed with the aim of assisting in the treatment of water with these metals [7; 9]. Carbon nanotubes (CNTs) have been an option and have been cited as adsorbent materials for heavy metals and their metabolites in contaminated waters [2; 9–12]. This is due to the fact that CNTs have a large surface area with one hydrophobic side and another easily modifiable with specific groups [2; 13]. Therefore, they can interact in various ways with heavy metals, such as electrostatic interactions, hydrophobic effects, and covalent bonds [14; 15].

However, the main difficulties for the application of CNTs are their suspension in treated solutions, pollution caused by chemicals used in functionalization, and high production costs [2]. Therefore, such materials have been reconsidered in future studies for large-scale application. Due to this, new structures formed by covalent bonds between benzene rings called cycloparaphenylenes or carbon nanobelts (CNBs) [16; 17] have been proposed as alternatives. These nanobelts have been investigated as an alternative structure for applications in various areas, since they have a highly delocalized electronic structure with sp^2 hybridization [18; 19], becoming attractive molecules by offering new possibilities for the synthesis of materials with different functional groups and serving as a template or seeds for the synthesis of other structures [18–20]. In addition, CNBs exhibit properties that can be exploited

*Corresponding authors

Email addresses: nike@hpqc.org (N. Dattani^{2,3}), icamps@unifal-mg.edu.br (I. Camps^{1,3})

when the belt acquires a Möbius topology, the Möbius carbon nanobelt (MCNBs), where the “twisted” structure should exhibit different molecular properties and movements compared to that with a normal belt topology [21; 22]. Studies show that CBNs and MCNBs exhibit specific fluorescence and chirality with possible use in optoelectronic optical materials [19; 22–25] and non-linear applications such as imaging and optical sensors [19; 22; 26].

Thinking about this, properties originating from different topologies can provide an alternative to solving current problems such as water pollution caused by chemical contaminants that generate adverse effects on nature and living organisms [3; 27].

In this study, the interaction of Cadmium (Cd), Nickel (Ni), and Lead (Pb), with carbon and Möbius-type carbon nanobelts were investigated using the semiempirical tight binding theory. Several methods were used to characterize the systems: best interaction region detection, geometry optimization, molecular dynamics, electronic property calculations, and topology studies.

2. Materials and Methods

In this work, four different types of four-atom metallic (M4) nanoclusters are studied interacting with two different types of carbon nanobelts. Structures of cadmium, nickel and lead clusters were created in the form of a linear (1DL) and a zigzag (1DZ) one-dimensional chains, a planar bi-dimensional (2D) structure and a tetrahedron three-dimensional (3D) and were put to interact with two types of carbon nanostructures: one consisting on a nanobelt and the other consisting on a Möbius nanobelt (twisted nanobelt). Starting with 2 units of a (10,0) carbon nanosheet repeated 10 times in the z direction and then wrapped 360 degrees, the nanobelts were generated using the Virtual NanoLab Atomistix Toolkit software [28]. Then, the periodicity was removed, and the surface was passivated with hydrogen atoms. For the Möbius nanobelts, after the initial repetition of the cells, the nanobelt was twisted 180 degrees and then wrapped. The structures of the metal nanoclusters, the carbon nanobelt (CNB) and Möbius carbon nanobelt (MCNB) are shown in Figure 1.

We utilized the semiempirical tight binding method to carry out the calculations, which were executed using the xTB program [29; 30]. The steps involved in the calculations are

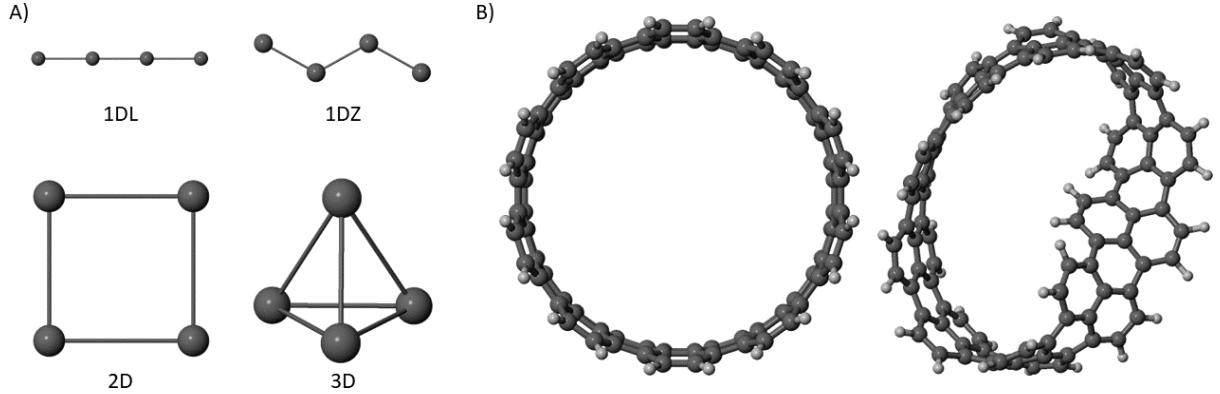


Figure 1: Initial structures. Panel A: metal nanoclusters. Panel B: carbon nanobelt (left), and Möbius carbon nanobelt (right).

explained in detail below.

Initially, the structures of every single system (comprising two nanobelts and four nanoclusters for each metal) were optimized. After that, we employed the automated Interaction Site Screening (aISS) [31] to create various intermolecular geometries such as CNB+M4 and MCNB+M4. These geometries were subsequently optimized, where they were ranked using the interaction energy (xTB-IFF) [32]. The genetic optimization step was carried out ten times until the best (lowest interaction energy) complex was obtained. The top-ranked complexes then underwent structural optimization. To evaluate the stability of the complexes, each structure from the aISS step underwent a molecular dynamic (MD) simulation for 100 ps. The parameters used in geometry optimizations are described in ref. [33].

The calculated electronic properties comprised the system energy, the highest occupied molecular orbital energy (HOMO, ε_H), the lowest unoccupied molecular orbital energy (LUMO, ε_L), the energy gap between the HOMO and LUMO orbitals ($\Delta\varepsilon = \varepsilon_H - \varepsilon_L$), and the atomic charges, which were determined using the CM5 scheme [34]. Using the computed charges, we estimated the charge transfer between the nanobelts and the isolated metal nanocluster by utilizing the following expression

$$\Delta Q_{M4} = Q_{M4}^{ads} - Q_{M4}^{iso}, \quad (1)$$

where Q_{M4}^{ads} is the total charge on the metal nanocluster after adsorption, and Q_{M4}^{iso} is the total charge for the isolated metal nanocluster.

We computed the binding energies (E_b) of the metals adsorbed on the nanobelts using the subsequent expression:

$$E_b = E_{NB+M4} - E_{NB} - E_{M4}. \quad (2)$$

In equation 2, E_{NB} and E_{M4} are the energies for the isolated nanobelts and metal nanoclusters, respectively, and E_{NB+M4} is the energy of the NB+M4 complex (CNB+M4 and MCNB+M4 systems).

The MULTIWFN [35] software was employed to determine the topological properties and descriptors (such as critical points, electronic density, Laplacian of the electronic density, etc.).

3. Results and discussion

3.1. Nanoclusters adsorption at the BN nanobelts

The fully relaxed structures are displayed in Figure 2. Among both nanobelts, the Cd1DL, Ni2D, and Pb2D nanoclusters exhibited the lowest energy complexes. Upon initial observation, the interaction with nickel nanoclusters caused more deformation in the nanobelts compared to the other metals, and also resulted in more bonds. Both of these tendencies may suggest that there is stronger binding between CNB and MCNB with Ni.

One of the primary differences between chemisorption and physisorption is their effect on the electronic states of both the adsorbate and the adsorbent [37]. Sections 3.2, and 3.3 will show that the electronic properties of the systems are modified after adsorption, which confirms this phenomenon.

Table 1 presents the data for the complexes with the lowest energy. The table reports two binding energies: E_b^{aISS} and E_b . The former is obtained from the aISS step, while the latter is calculated using equation 2 for the fully optimized individual structures and the final complex. Upon comparing both binding energies for each system, it is observed

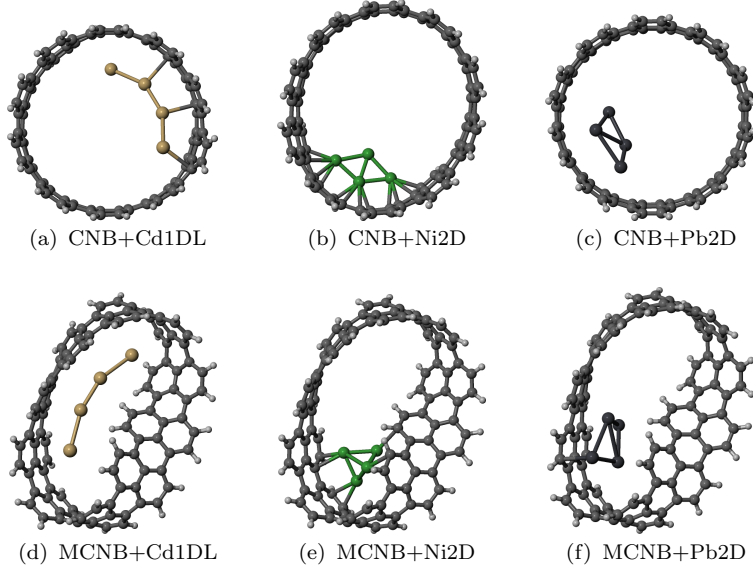


Figure 2: Fully relaxed complexes with lowest energies. Image rendered with Jmol software [36].

Table 1: Electronic and bond distances from optimized geometries[†].

| Complex | E_b^{aISS} | E_b | ΔQ_M | Gap ($\Delta\varepsilon$) | Distances |
|------------|--------------|---------|--------------|-----------------------------|---|
| CNB+Cd1DL | -77.29 | -59.38 | 0.1517 | 0.632 | 2.79/2.80/2.81/3.06/3.10 |
| CNB+Ni2D | -136.25 | -123.79 | -0.7671 | 0.158 | 2.36(2)/2.37(2)/2.38(2)/2.43(2) |
| CNB+Pb2D | -100.83 | -61.78 | 0.3862 | 0.039 | 2.84/2.86/3.74 |
| MCNB+Cd1DL | -91.74 | -77.91 | 0.2328 | 0.543 | 2.80/3.00/3.01/3.14 3.23/3.27/3.36/3.41/3.45 |
| MCNB+Ni2D | -158.77 | -146.30 | -0.7426 | 0.101 | 2.35/2.37/2.42/2.44/2.45 |
| MCNB+Pb2D | -118.60 | -79.56 | 0.8055 | 0.495 | 2.41/2.67/2.68/2.76/2.80/3.32/3.58 |

[†] E_b^{aISS} and E_b are in units kcal/mol, ΔQ_M are in units of e , $\Delta\varepsilon$ is in units of eV and the distances are in units of \AA , respectively.

that the Ni₂D nanocluster has the lowest binding energies for both nanobelts, which suggests stronger adsorption. The binding energy (E_b) for Cd₁DL and Pb₂D clusters are very similar with a difference around 2 kcal/mol. Since all the binding energies are negative, it can be inferred that all the adsorption processes are favorable.

The visual depiction of the complexes in Figure 2 suggests that only Cd and Ni established bonds with the nanobelts. Specifically, Cd formed three bonds with CNB and none with MCNB, while the Ni cluster formed twelve bonds with CNB and six with MCNB. In contrast, Pb did not establish any bonds with either CNB or MCNB. However, since the bond information from Figure 2 is solely based on geometrical data, the Quantum Theory of Atoms in Molecule (QTAIM) [38] was employed in Section 3.3 as a more precise method to examine bond formation.

Geometry optimization entails utilizing an algorithm to acquire a local minimum structure on the potential energy surface (PES) to determine the lowest energy conformers of a system. However, this approach does not offer any insights into the system’s stability over time. In contrast, molecular dynamics simulation examines the motion of atoms and molecules at a specific temperature (in this case, 298.15 K) and provides a way to explore the PES. We utilized this method to perform simulations on each complex, starting with the structures obtained from the aISS step as initial conformations. The simulations were conducted for a production time frame of 100 ps with a time step of 2 fs and an optional dump step of 50 fs, at which the final structure was saved to a trajectory file.

In Figures 3 and 4, panel A displays the root-mean-square deviation (RMSD) of the metal nanoclusters, while panel B shows the system frames at various simulation times (0 ps, 25 ps, 50 ps, 75 ps, and 100 ps). The low RMSD values ($< 2 \text{ \AA}$) suggest that the metal nanocluster conformations remained relatively constant, indicating structural stability. By comparing the figures’ snapshots with Figure 1B, we confirmed that the Ni nanocluster caused the most significant changes to the nanobelt. From panel B, it is apparent that the metal nanoclusters remained bound to their corresponding carbon nanobelts in all cases, indicating complex stability. This is confirmed by the negative binding energy during the simulation time as shown in Figure 5. The full molecular dynamics movies can be

downloaded from the Zenodo server [39].

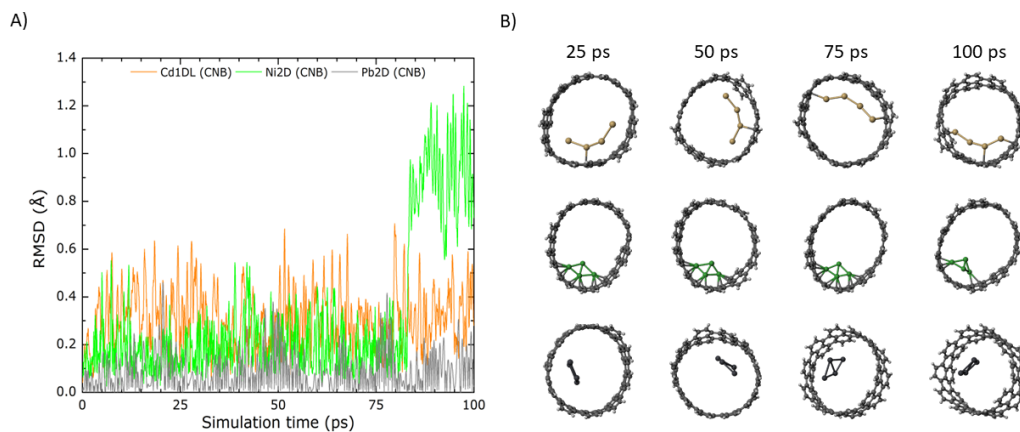


Figure 3: Panel A: Calculated RMSD for metal nanocluster from CNB complexes. Panel B: Snapshots of CNB complexes at different simulation times.

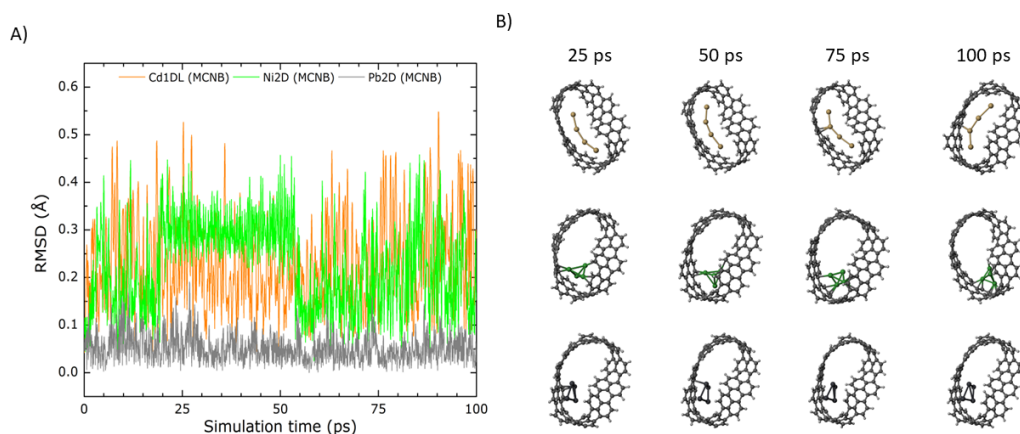


Figure 4: Panel A: Calculated RMSD for metal nanocluster from MCNB complexes. Panel B: Snapshots of MCNB complexes at different simulation times.

3.2. Electronic properties

Figures 6 and 7 show the calculated highest occupied/lowest unoccupied molecular orbitals (HOMO/LUMO) for all optimized systems.

The molecular orbitals for the CNB system (Figures 6(a) and 7(a)) are homogeneously distributed over the entire structure, as expected due to the belt symmetry. Surprisingly,

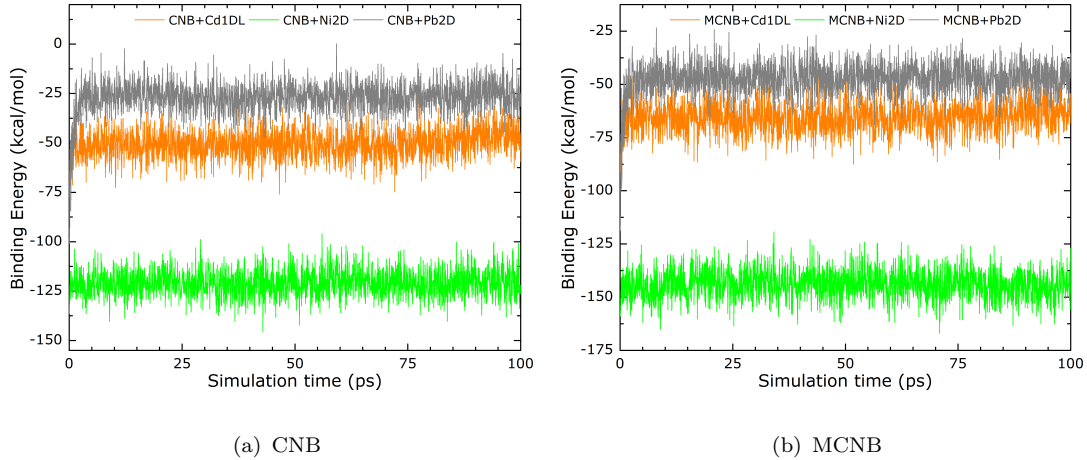


Figure 5: Binding energy of CNB and MCNB complexes during the simulation time.

despite the symmetry break due to the twist, the HOMO and LUMO distribution for MCNB (Figures 6(e) and 7(e)) remain almost homogeneously distributed over the Möbius carbon nanobelt. This behavior is in contrast what happens for Möbius boron–nitride nanobelt where the HOMO/LUMO distributions are affected by the twist [40].

Figures 6 and 7 depict the HOMO/LUMO molecular orbitals for all optimized systems. The CNB system’s molecular orbitals (Figures 6(a) and 7(a)) are distributed uniformly throughout the structure, as expected due to the symmetry of the belt. Surprisingly, despite the symmetry break caused by the twist, the HOMO and LUMO distribution for MCNB (Figures 6(e) and 7(e)) remain almost uniformly distributed over the Möbius carbon nanobelt. The finding presented here is in contrast to the behavior of Möbius boron–nitride nanobelts, where the twist affects the HOMO/LUMO distributions, as reported in our previous study [40]. This indicates that the electron distribution in carbon nanobelts is more flexible or “plastic” compared to boron–nitride nanobelts. The electronic gap for the CNB is equal to 0.449 eV, which is slightly decreased to 0.352 eV for the MCNB.

When metal nanoclusters bind to carbon nanobelts, it causes a slight decrease in the volume of the frontier orbitals on the nanobelt’s surface, with the most significant decrease observed for Ni, followed by Cd and then Pb. This is unlike what occurs when the same metal nanoclusters interact with boron–nitride nanobelts, where the binding drastically changes

the orbital surface distribution [40]. Additionally, the interaction between the nanobelts and the metals increases the volume of the orbitals surfaces around the regions where the metals are bonded. The interaction of both nanobelts with all the metals modified the gap, as shown in Table 1. The greatest charge transfer (ΔQ_{M4}) between the nanobelts and the nanoclusters occurred in the case of Ni for both CNB and MCNB. Based on the significant modifications observed in the electronic properties of the CNB and MCNB after interaction with metals, it can be concluded that chemisorption occurs for all systems.

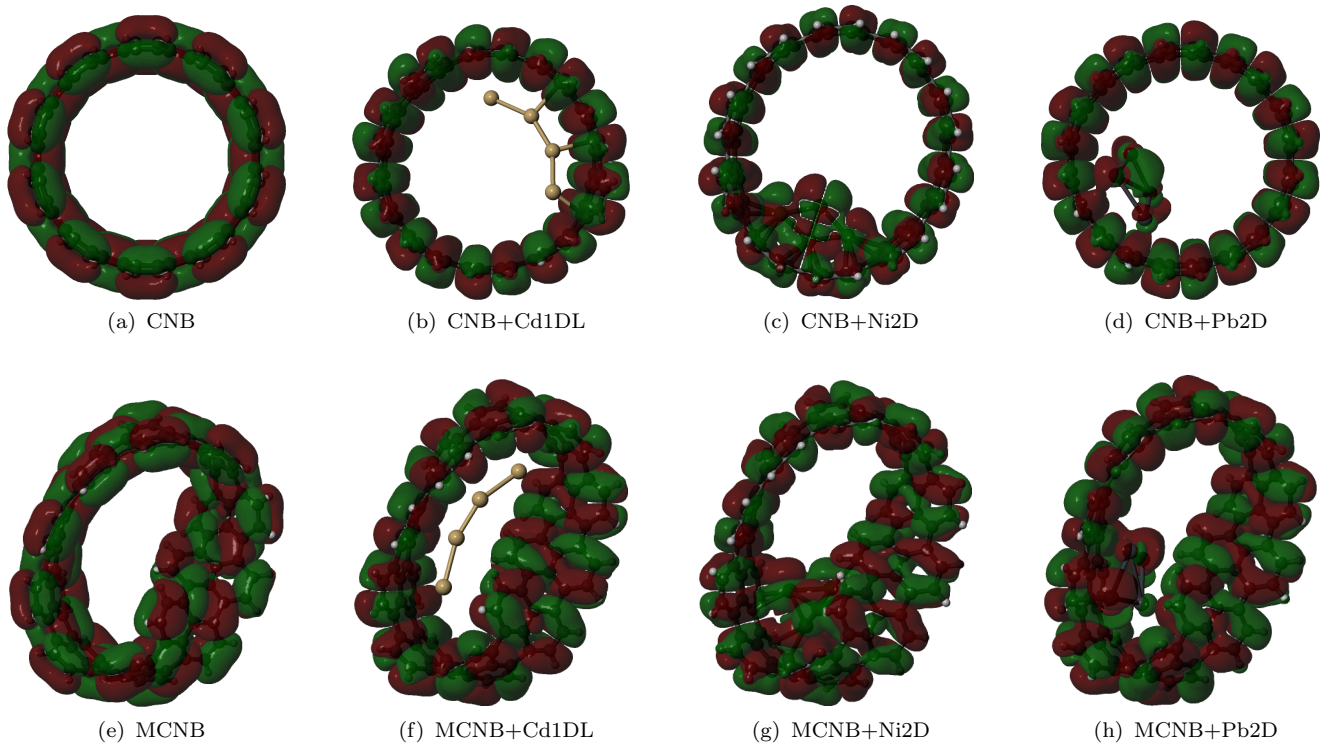


Figure 6: Highest occupied molecular orbital (HOMO) for all systems. Red (green) color represents negative (positive) values. Orbital surfaces rendered with with isovalue equal to 0.001 and with Jmol software [36].

3.3. Topological analysis

The aim of topological analysis is to detect critical points, which are positions where the gradient norm of the electron density value equals zero. The critical points are categorized into four types based on the negative eigenvalues of the Hessian matrix of the real function [38]. The criteria for bond classification and types of critical points are described in

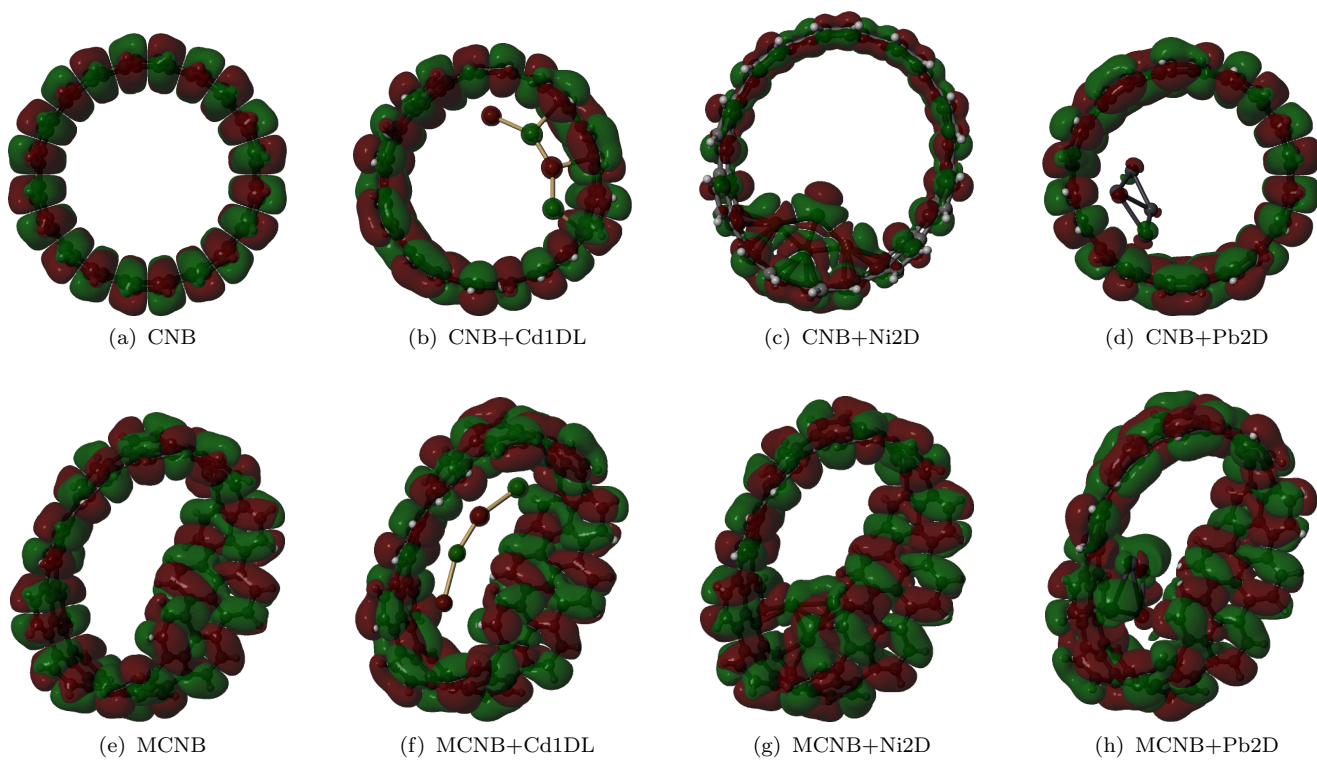


Figure 7: Lowest unoccupied molecular orbital (LUMO) for all systems. Red (green) color represents negative (positive) values. Orbital surfaces rendered with with isovalue equal to 0.001 and with Jmol software [36].

detail in ref. [33].

Figure 8 show the critical points for each complex. The orange dots represent the bond critical points (BCPs), the yellow dots represent the ring critical points (RCPs), and the green dots represent the cage critical points (CCPs). All the complexes show several critical points, indicating a favorable interaction between the metals and the belts. In all cases, the number of critical points made between the metal nanocluster and the Möbius nanobelts is greater than with the nanobelts alone. This can be associated with the fact that Möbius belts form like small pockets where the metal nanocluster can be docked. The interaction between the metal nanocluster with the MCNB create bonds with both sides of the pocket. For better visualization of the formed critical points, movies with spinning structures can be downloaded from the Zenodo server [39]. Another confirmation that the strongest interactions are between the Ni nanoclusters and the carbon nanobelts is the lowest bond distances shown in Table 1.

Figure 8 displays the critical points for each complex, with the bond critical points (BCPs) represented by orange dots, the ring critical points (RCPs) represented by yellow dots, and the cage critical points (CCPs) represented by green dots. The presence of multiple critical points in all complexes indicates a favorable interaction between the metals and the belts. Moreover, the number of critical points formed between the metal nanocluster and the Möbius nanobelts is higher than those formed between the nanobelts alone, which can be attributed to the small pockets formed by the Möbius belts that allow for the metal nanocluster to dock. The interaction between the metal nanocluster and the MCNB leads to bonds formed on both sides of the pocket. For better visualization of the formed critical points, spinning structure movies can be downloaded from the Zenodo server [39]. The lowest bond distances shown in Table 1 provide additional evidence that the strongest interactions occur between the Ni nanoclusters and the carbon nanobelts.

The use of ρ and $\nabla^2\rho$ values and indexes such as ELF and LOL can provide insight into the bond type (covalent or non-covalent) in various systems. The localization of electron movement is related to the ELF index, which ranges from 0 to 1 [42; 43]. High values of the ELF index indicate a high degree of electron localization, which suggests the presence of a

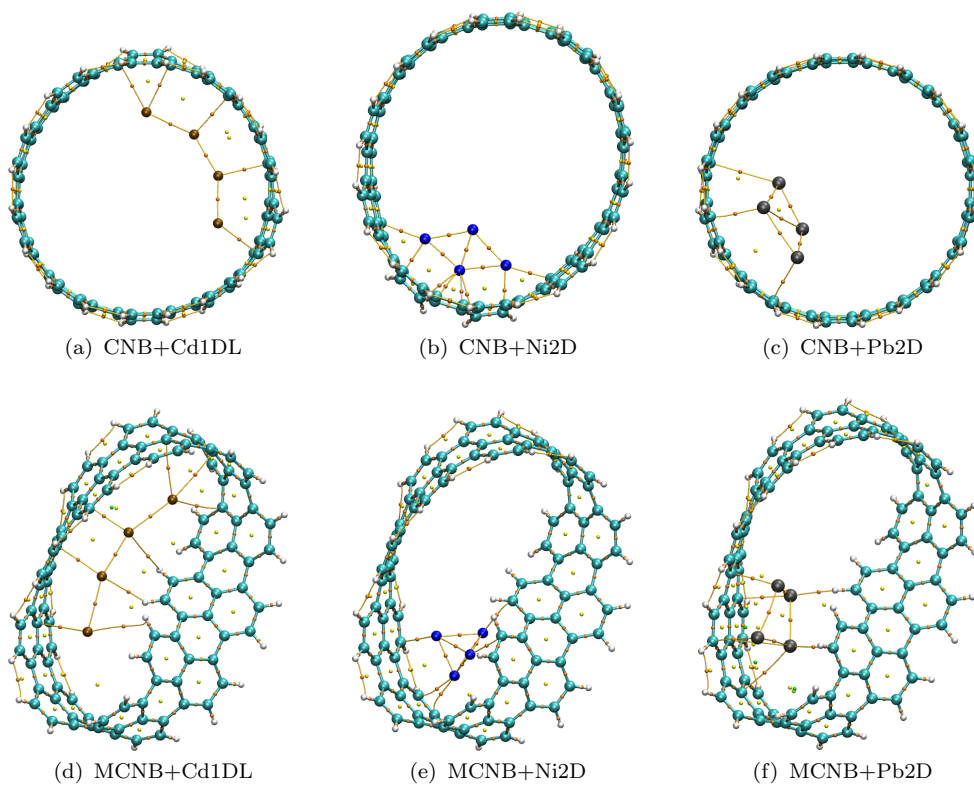


Figure 8: Critical points: BCPs, RCPs and CCPs (orange, yellow, and green dots, respectively). Image rendered with VMD software [41].

covalent bond. The LOL index is another function that can be used to identify regions of high localization [44]. The LOL index also ranges from 0 to 1, with smaller (larger) values usually occurring in the boundary (inner) regions.

Figure 9 shows the electron density (ρ), Laplacian of the electron density ($\nabla^2\rho$), electron localization function (ELF) index, and localized orbital locator (LOL) index at all the detected bond critical points. The values of BCPs descriptors for MCNB is greater than for CNB, indicating that using Möbius carbon nanobelts to capture heavy metal nanoclusters is a better choice.

As higher values of ρ can be an indicator of the strength of the bond, Figures 9(a), 9(b), 9(e), and 9(f) show that MCNB made stronger bonds with Ni than with Cd or Pb (green, orange and gray regions, respectively). Even though Cd nanocluster forms more bonds with MCNB than Ni nanocluster, they have, in general, lower values of ρ and $\nabla^2\rho$ except for one bond. The ELF (figures 9(c), and 9(g)) and LOL (figures 9(d), and 9(h)) indexes show that only one Cd bond critical point has greater values than for Ni and Pb clusters. The topological analysis confirms that both carbon nanobelts are capable of adsorbing the three heavy metal nanoclusters studied here. Nevertheless, the MCNB presented greater values for all the descriptors used. In all cases, the Ni nanoclusters are chemisorbed, whereas Cd and Pb nanoclusters are physisorbed.

Figure 9 displays several indexes related to the electron density and its confinement, such as the electron localization function (ELF) and localized orbital locator (LOL) index, for all the identified bond critical points. The descriptors for bond critical points (BCPs) are greater for Möbius carbon nanobelts (MCNB) compared to conventional carbon nanobelts (CNB), indicating that MCNB is more suitable for capturing heavy metal nanoclusters. The figures of the electron density (ρ) and Laplacian of the electron density ($\nabla^2\rho$), Figures 9(a),9(b),9(e), and 9(f), show that MCNB makes stronger bonds with Ni than with Cd or Pb, as shown by the larger bars of green, orange, and gray colors, respectively. While Cd nanocluster forms more bonds with MCNB than Ni nanocluster, their values of ρ and $\nabla^2\rho$ are generally lower, except for one bond. The ELF and LOL indexes for Figures 9(c),9(g),9(d), and 9(h) reveal that only one Cd bond critical point has greater values than the critical points descriptors

for Ni and Pb clusters. The analysis indicates that both types of carbon nanobelts can adsorb the three heavy metal nanoclusters studied here. Nonetheless, MCNB shows greater values for all the descriptors used. In all cases, Ni nanoclusters are chemisorbed, whereas Cd and Pb nanoclusters are physisorbed.

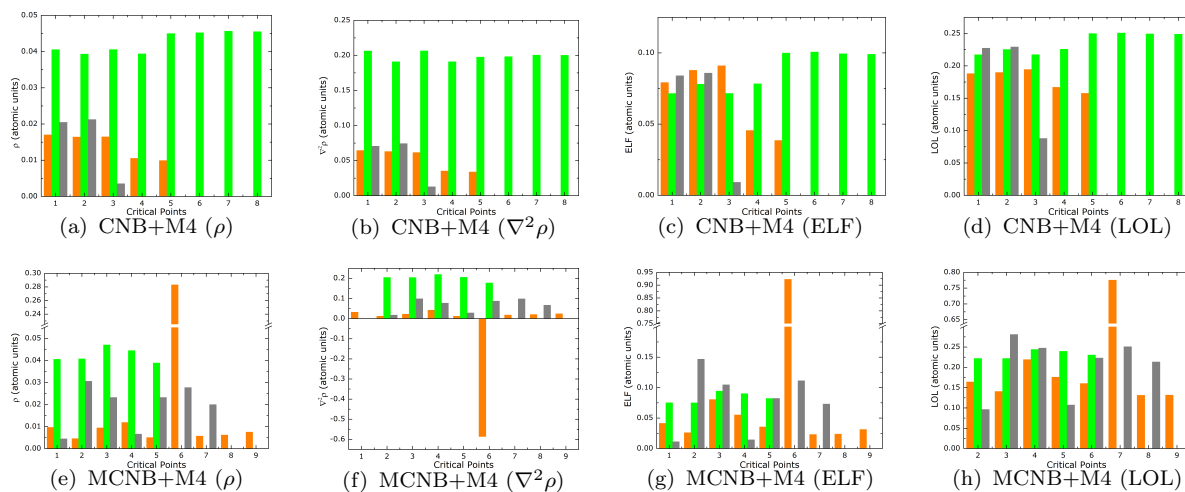


Figure 9: Topology results for Ni, Cd and Pb nanoclusters are shown in green, orange and gray, respectively.

4. Conclusions

This study investigated the interactions between Ni, Cd, and Pb nanoclusters and carbon nanobelts with different geometries. Various methods were used, including the automated Interaction Site Screening (aISS) to identify the best interaction regions, geometry optimization, molecular dynamics simulations, electronic property calculations, and topological analysis.

The optimized structures were used to calculate the binding energy for each complex, and the results indicated that the Ni nanocluster showed the most favorable interaction followed by Pb and Cd nanoclusters. Molecular dynamics simulations showed that the heavy metals remained bound to the nanobelts with negative binding energy during the production time of 100 ps.

The electronic calculations revealed that the topology of the MCNB slightly altered the HOMO/LUMO distribution, indicating good electron mobility. The HOMO/LUMO surfaces

were redistributed around the region where the metal was located due to the metal/nanobelt interaction. Moreover, the Ni nanocluster caused a more significant modification of the nanocluster's charges than the other metals.

The topological analysis identified the critical points that helped characterize the type and strength of the interactions. The MCNB had higher values for all descriptors than the CNB systems, indicating that using MCNB to adsorb heavy metals is a better choice. The Ni nanocluster was better adsorbed than the Cd and Pb nanoclusters, as indicated by the values of the descriptors used (electron density, Laplacian of the electron density, ELF, and LOL indexes).

Overall, combining the results from geometry optimization, binding energy calculation, and topological analysis, the study concluded that Ni nanoclusters are chemisorbed, while Cd and Pb nanoclusters are physisorbed in both nanobelts, with more favorable adsorption for the Möbius carbon nanobelts.

CRedit authorship contribution statement

C. Aguiar: Investigation, Formal analysis, Writing–original draft, Writing–review & editing. **N. Dattani:** Investigation, Resources, Formal analysis, Writing–original draft, Writing–review & editing. **I. Camps:** Conceptualization, Methodology, Software, Formal analysis, Resources, Writing–review & editing, Supervision, Project administration.

Declaration of competing interest

The authors declare that they have no known competing financial interests or personal relationships that could have appeared to influence the work reported in this paper.

Data availability

The raw data required to reproduce these findings are available to download from <https://doi.org/10.5281/zenodo.7823747>.

Acknowledgements

We would like to acknowledge financial support from the Brazilian agencies CNPq, CAPES and FAPEMIG. Part of the results presented here were developed with the help of a CENAPAD-SP (Centro Nacional de Processamento de Alto Desempenho em São Paulo) grant UNICAMP/FINEP-MCT, CENAPAD-UFC (Centro Nacional de Processamento de Alto Desempenho, at Universidade Federal do Ceará), and Digital Research Alliance of Canada (via project bmh-491-09 belonging to Dr. Nike Dattani), for the computational support.

References

- [1] R. Kumar, M. A. Khan, N. Haq, Application of carbon nanotubes in heavy metals remediation, *Crit. Rev. Env. Sci. Tec.* 44 (2014) 1000–1035 (2014). doi:10.1080/10643389.2012.741314.
- [2] A. T. Hoang, S. Nizetić, C. K. Cheng, R. Luque, S. Thomas, T. L. Banh, V. V. Pham, X. P. Nguyen, Heavy metal removal by biomass-derived carbon nanotubes as a greener environmental remediation: A comprehensive review, *Chemosphere* 287 (2022) 131959 (2022). doi:10.1016/j.chemosphere.2021.131959.
- [3] R. Baby, B. Saifullah, M. Z. Hussein, Carbon nanomaterials for the treatment of heavy metal-contaminated water and environmental remediation, *Nanoscale Res. Lett.* 14 (2019) 341 (2019). doi:10.1186/s11671-019-3167-8.
- [4] C. Zamora-Ledezma, D. Negrete-Bolagay, F. Figueroa, E. Zamora-Ledezma, M. Ni, F. Alexis, V. H. Guerrero, Heavy metal water pollution: A fresh look about hazards, novel and conventional remediation methods, *Environ. Technol. Innov.* 22 (2021) 101504 (2021). doi:10.1016/j.eti.2021.101504.
- [5] I. M. Kolangare, A. M. Isloor, Inamuddin, A. M. Asiri, A. F. Ismail, Improved desalination by polyamide membranes containing hydrophilic glutamine and glycine, *Environ. Chem. Lett.* 17 (2018) 1053–1059 (2018). doi:10.1007/s10311-018-00825-1.
- [6] A. Zwolak, M. Sarzyńska, E. Szpyrka, K. Stawarczyk, Sources of soil pollution by heavy metals and their accumulation in vegetables: A review, *Water, Air, Soil Pollution* 230 (2019) 1–9 (2019). doi:10.1007/s11270-019-4221-y.
- [7] A. T. Hoang, X. D. Pham, An investigation of remediation and recovery of oil spill and toxic heavy metal from maritime pollution by a new absorbent material, *J. Mar. Eng. Technol.* 20 (2018) 159–169 (2018). doi:10.1080/20464177.2018.1544401.
- [8] M. S. Schuler, R. A. Relyea, A review of the combined threats of road salts and heavy metals to freshwater systems, *BioScience* 68 (2018) 327–335 (2018). doi:10.1093/biosci/biy018.
- [9] B. Arora, P. Attri, Carbon nanotubes (CNTs): A potential nanomaterial for water purification, *J. Compos. Sci.* 4 (2020) 135 (2020). doi:10.3390/jcs4030135.
- [10] H. Moallaei, J.-P. Bouchara, A. Rad, P. Singh, P. Raizada, H. N. Tran, M. N. Zafar, D. A. Gianakoudakis, A. Hosseini-Bandegharai, Application of *fusarium sp.* Immobilized on multi-walled carbon nanotubes for solid-phase extraction and trace analysis of heavy metal cations, *Food Chem.* 322 (2020) 126757 (2020). doi:10.1016/j.foodchem.2020.126757.
- [11] M. A. Ganzoury, C. Chidiac, J. Kurtz, C.-F. de Lannoy, CNT-sorbents for heavy metals: Electrochemical regeneration and closed-loop recycling, *J. Hazard. Mater.* 393 (2020) 122432 (2020). doi:10.1016/j.jhazmat.2020.122432.
- [12] A. R. Oliveira, A. A. Correia, M. G. Rasteiro, Heavy metals removal from aqueous solutions by multiwall

- carbon nanotubes: effect of MWCNTs dispersion, *Nanomaterials* 11 (2021) 2082 (2021). doi:10.3390/nano11082082.
- [13] B. O. Murjani, P. S. Kadu, M. Bansod, S. S. Vaidya, M. D. Yadav, Carbon nanotubes in biomedical applications: current status, promises, and challenges, *Carbon Letters* 32 (2022) 1207–1226 (2022). doi:10.1007/s42823-022-00364-4.
- [14] M. J. S. Treviño, S. Zarazúa, J. Płotka-Wasyłka, Nanosorbents as materials for extraction processes of environmental contaminants and others, *Molecules* 27 (2022) 1067 (2022). doi:10.3390/molecules27031067.
- [15] K. Pyrzynska, Recent applications of carbon nanotubes for separation and enrichment of lead ions, *Separations* 10 (2023) 152 (2023). doi:10.3390/separations10030152.
- [16] G. Povie, Y. Segawa, T. Nishihara, Y. Miyauchi, K. Itami, Synthesis of a carbon nanobelt, *Science* 356 (2017) 172–175 (2017). doi:10.1126/science.aam8158.
- [17] S. Nishigaki, Y. Shibata, A. Nakajima, H. Okajima, Y. Masumoto, T. Osawa, A. Muranaka, H. Sugiyama, A. Horikawa, H. Uekusa, H. Koshino, M. Uchiyama, A. Sakamoto, K. Tanaka, Synthesis of belt- and Möbius-shaped cycloparaphenylenes by rhodium-catalyzed alkyne cyclotrimerization, *J. Am. Chem. Soc.* 141 (2019) 14955–14960 (2019). doi:10.1021/jacs.9b06197.
- [18] Q. Zhang, Y.-E. Zhang, S. Tong, M.-X. Wang, Hydrocarbon belts with truncated cone structures, *J. Am. Chem. Soc.* 142 (2020) 1196–1199 (2020). doi:10.1021/jacs.9b12181.
- [19] N. Li, L. Zhang, C. Lu, Y. Sun, J. Wang, Physical mechanism of spectra in carbon nanobelts under quantum size effect, *Nanomaterials* 13 (2022) 159 (2022). doi:10.3390/nano13010159.
- [20] S. Seenithurai, J.-D. Chai, Electronic properties of carbon nanobelts predicted by thermally-assisted-occupation DFT, *Nanomaterials* 11 (2021) 2224 (2021). doi:10.3390/nano11092224.
- [21] D. Ajami, O. Oeckler, A. Simon, R. Herges, Synthesis of a Möbius aromatic hydrocarbon, *Nature* 426 (2003) 819–821 (2003). doi:10.1038/nature02224.
- [22] Y. Segawa, T. Watanabe, K. Yamanoue, M. Kuwayama, K. Watanabe, J. Pirillo, Y. Hijikata, K. Itami, Synthesis of a Möbius carbon nanobelt, *Nature Synthesis* 1 (2022) 535–541 (2022). doi:10.1038/s44160-022-00075-8.
- [23] C. Wu, W. Liu, K. Li, G. Cheng, J. Xiong, T. Teng, C.-M. Che, C. Yang, Face-to-face orientation of quasiplanar donor and acceptor enables highly efficient intramolecular exciplex fluorescence, *Angew. Chem. Int. Ed.* 60 (2020) 3994–3998 (2020). doi:10.1002/anie.202013051.
- [24] W. Li, C.-Z. Du, X.-Y. Chen, L. Fu, R.-R. Gao, Z.-F. Yao, J.-Y. Wang, W. Hu, J. Pei, X.-Y. Wang, BN-anthracene for high-mobility organic optoelectronic materials through periphery engineering, *Angew. Chem. Int. Ed.* 61 (2022). doi:10.1002/anie.202201464.
- [25]

- [26] R. Li, Y. Zhang, X. Xu, Y. Zhou, M. Chen, M. Sun, Optical characterizations of two-dimensional materials using nonlinear optical microscopies of CARS, TPEF, and SHG, *Nanophotonics* 7 (2018) 873–881 (2018). doi:10.1515/nanoph-2018-0002.
- [27] Y. Wu, H. Pang, Y. Liu, X. Wang, S. Yu, D. Fu, J. Chen, X. Wang, Environmental remediation of heavy metal ions by novel-nanomaterials: A review, *Environ. Pollut.* 246 (2019) 608–620 (2019). doi:10.1016/j.envpol.2018.12.076.
- [28] Virtual NanoLab - Atomistix ToolKit. QuantumWise. v2017.1 (2017).
- [29] C. Bannwarth, E. Caldeweyher, S. Ehlert, A. Hansen, P. Pracht, J. Seibert, S. Spicher, S. Grimme, Extended tight-binding quantum chemistry methods, *WIREs Comput. Mol. Sci.* 11 (2020) e1493 (2020). doi:10.1002/wcms.1493.
- [30] S. Grimme, C. Bannwarth, P. Shushkov, A robust and accurate tight-binding quantum chemical method for structures, vibrational frequencies, and noncovalent interactions of large molecular systems parametrized for all spd-block elements ($Z=1-86$), *J. Chem. Theory Comput.* 13 (2017) 1989–2009 (2017). doi:10.1021/acs.jctc.7b00118.
- [31] C. Plett, S. Grimme, Automated and efficient generation of general molecular aggregate structures, *Angew. Chem. Int. Ed.* 62 (2022). doi:10.1002/anie.202214477.
- [32] S. Grimme, C. Bannwarth, E. Caldeweyher, J. Pisarek, A. Hansen, A general intermolecular force field based on tight-binding quantum chemical calculations, *J. Chem. Phys.* 147 (2017) 161708 (2017). doi:10.1063/1.4991798.
- [33] I. Camps, Methods used in nanostructure modeling (2023). doi:10.48550/arXiv.2303.01226.
- [34] A. V. Marenich, S. V. Jerome, C. J. Cramer, D. G. Truhlar, Charge Model 5: an extension of Hirshfeld population analysis for the accurate description of molecular interactions in gaseous and condensed phases, *Journal of Chemical Theory and Computation* 8 (2012) 527–541 (2012). doi:10.1021/ct200866d.
- [35] T. Lu, F. Chen, Multiwfn: A multifunctional wavefunction analyzer, *J. Comput. Chem.* 33 (2012) 580–592 (2012). doi:10.1002/jcc.22885.
- [36] Jmol: An open-source Java viewer for chemical structures in 3D. <http://www.jmol.org/>.
- [37] D. H. Everett, Manual on Definitions, Terminology and Symbols in Colloid and Surface Chemistry (internet version), Vol. 31, IUPAC. Division of Physical Chemistry, 2001 (2001). doi:10.1351/pac197231040577.
- [38] Richard F. W. Bader, *Atoms in Molecules: A Quantum Theory*, Clarendon Press, 1994 (1994).
- [39] C. Aguiar, N. Dattani, I. Camps, (VIDEOS) Möbius carbon nanobelts interacting with heavy metal nanoclusters (2023). doi:10.5281/zenodo.7821847.
- [40] C. Aguiar, N. Dattani, I. Camps, Möbius boron–nitride nanobelts interacting with heavy metal nan-

- oclusters (2023). doi:10.48550/arXiv.2302.11697.
- [41] W. Humphrey, A. Dalke, K. Schulten, VMD: Visual molecular dynamics, *Journal of Molecular Graphics* 14 (1996) 33–38 (fe 1996). doi:10.1016/0263-7855(96)00018-5.
- [42] A. D. Becke, K. E. Edgecombe, A simple measure of electron localization in atomic and molecular systems, *The Journal of Chemical Physics* 92 (1990) 5397–5403 (1990). doi:10.1063/1.458517.
- [43] K. Koumpouras, J. A. Larsson, Distinguishing between chemical bonding and physical binding using electron localization function (ELF), *J. Phys.: Condens. Matter* 32 (2020) 315502 (2020). doi:10.1088/1361-648X/ab7fd8.
- [44] H. L. Schmider, A. D. Becke, Chemical content of the kinetic energy density, *J. Mol. Struct.: THEOCHEM* 527 (2000) 51–61 (2000). doi:10.1016/S0166-1280(00)00477-2.